

A Recurrent Spiking Network with Hierarchical Intrinsic Excitability Modulation for Schema Learning

Yingchao Yu^a, Yaochu Jin^{*b}, Yuchen Xiao^c, Yuping Yan^b

^a*College of Information Science and Technology, Donghua University, No. 2999 Renmin North Road, Songjiang District, Shanghai, 201620, Shanghai, China*

^b*School of Engineering, Westlake University, 600 Dunyu Road, Xihu District, Hangzhou, 310030, Zhejiang, China*

^c*School of Life Sciences, Westlake University, 600 Dunyu Road, Xihu District, Hangzhou, 310030, Zhejiang, China*

Abstract

Schema, a form of structured knowledge that promotes transfer learning, is attracting growing attention in both neuroscience and artificial intelligence (AI). Current schema research in neural computation is largely constrained to a single behavioral paradigm and relies heavily on recurrent neural networks (RNNs) which lack the neural plausibility and biological interpretability. To address these limitations, this work first constructs a generalized behavioral paradigm framework for schema learning and introduces three novel cognitive tasks, thus supporting a comprehensive schema exploration. Second, we propose a new model using recurrent spiking neural networks with hierarchical intrinsic excitability modulation (HM-RSNNs). The top level of the model selects excitability properties for task-specific demands, while the bottom level fine-tunes these properties for intra-task problems. Finally, extensive visualization analyses of HM-RSNNs are conducted to showcase their computational advantages, track the intrinsic excitability evolution during schema learning, and examine neural coordination differences across tasks. Biologically inspired lesion studies further uncover task-specific distributions of intrinsic excitability within schemas. Experimental results show that HM-RSNNs significantly outperform RSNN baselines across all tasks and exceed RNNs in three novel cognitive tasks. Additionally, HM-RSNNs offer deeper insights into neural dynamics underlying schema learning.

^{*}Corresponding author. Email: jinyaochu@westlake.edu.cn

Keywords: Schema Learning, Recurrent Spiking Networks, Intrinsic Excitability

1. Introduction

Cognitive flexibility, a hallmark of biological intelligence, refers to the capacity for adapting thoughts and behaviors in dynamic or novel environments [1]. This adaptability is supported by schemas in the brain, which are abstract, structural knowledge formed through the integration and consolidation of past experiences [2, 3], enhancing generalization and supporting transfer learning [4, 5].

Current schema studies mainly base on biological experiments, with an emphasis on schema representation, including the disentanglement and organization of components [6], inter-regional cooperation across brain areas [7, 8], dynamic goal-progress tuning [9], and the evolution of representations during learning [5]. Compared to biological schema research, computational models present distinct advantages as they facilitate schema formation from scratch under controlled conditions, support a wider range of tasks at lower costs, provide full observability of internal states, and bridge the gap to artificial intelligence (AI) applications [10]. However, current computational schema studies remain limited, focusing on single cognitive tasks and relying primarily on continuous recurrent neural networks (RNNs) with their simplified node-like neurons. For example, Goudar et al. trained RNNs on sensorimotor tasks, showing that a low-dimensional neural subspace supports schema formation and accelerates learning in new tasks by reducing changes in connection weights [11].

By contrast, recurrent spiking neural networks (RSNNs) are gaining increasing attention due to their neural plausibility and biological interpretability [12, 13, 14, 15]. By leveraging neuronal dynamics and precise spike timing, RSNNs effectively model complex neural interactions, enabling more realistic brain simulations and offering deeper insights into neural processing [16]. However, modeling schema learning with RSNNs has not been explored, as training these nondifferentiable networks on complex cognitive tasks presents a significant challenge compared to continuous RNNs, often leading to sub-optimal performance [17].

In this work, we present the first attempt to model schema learning using RSNNs. We propose an advanced RSNN model with hierarchical modulation

of intrinsic excitability (HM-RSNN), addressing the learning limitations of RSNNs and enabling accurate modeling of schema learning. The modulation in HM-RSNNs acts as a metaplasticity mechanism, adjusting the biochemical state of neurons to optimize their properties for task-specific demands. Specifically, the modulation occurs at two levels: the top level, simulating the function of astrocytes, guides task-specific selection of intrinsic excitability properties, whereas the bottom level refines these selected properties for intra-task problem-solving.

Moreover, we construct a generalized schema learning framework based on the work in [11] and introduce three additional cognitive tasks, namely the Context-Dependent Delayed Match-to-Sample (CD-DMS) task and two Go/No-Go Delayed Recall (GNG-DR) tasks, GNG-DR-2 and GNG-DR-4, offering a systematic investigation of schema learning.

Finally, we perform comprehensive visualization analyses of HM-RSNNs to demonstrate their computational benefits, track the progression of intrinsic excitability during schema learning, and investigate differences in neural coordination across tasks. Additionally, biologically inspired lesion studies reveal task-specific distributions of intrinsic excitability within schemas. Our main contributions are as follows:

- A generalized schema learning framework with three additional cognitive tasks is constructed. To ensure methodological rigor, the data generation process is carefully designed to make the stimuli in each problem distinguishable and to keep the data across problems independent.
- An advanced RSNN model, named HM-RSNN, is proposed, incorporating a collaborative two level modulation mechanism to address the performance limitations of RSNNs in schema learning.
- Comprehensive experiments on four schema tasks are conducted, demonstrating that HM-RSNNs outperform vanilla RSNNs, other RSNN variants, and traditional RNN models, while adapting more effectively to abrupt changes and positioning themselves as a promising alternative to conventional RNNs.
- Extensive visualization and lesion analyses are performed, leveraging the biomimetic properties of HM-RSNNs to reveal characteristics in intrinsic excitability and neural coordination during schema learning.

The remainder of this article is structured as follows. Section 2 outlines the preliminaries. Section 3 elaborates on the generalized schema learning framework, the additional cognitive tasks, and the proposed HM-RSNNs. Section 4 presents the experimental studies. Section 5 concludes the paper with a discussion of its limitations.

2. Preliminaries

2.1. The vanilla RSNN model

This work makes the first attempt to simulate the brain's schema learning process using an RSNN model. RSNN dynamics are described below.

At each time step t , the membrane potential of neurons is given by:

$$V(t) = \alpha_s V(t-1) + (1 - \alpha_s)(\mathbf{W}_{\text{in}} X(t) + \mathbf{W}_{\text{rec}} S_{\text{mem}}(t-1) + N(t)), \quad (1)$$

where \mathbf{W}_{in} and \mathbf{W}_{rec} denote the input and recurrent weight matrices. $\alpha_s = \exp^{-\Delta t/\tau_s}$ is the decay factor for the somatic time constant τ_s . $X(t)$ is the input vector at time t , $S_{\text{mem}}(t-1)$ represents the membrane states of recurrent neurons at the previous time step, and $N(t)$ models brain-like noise that introduces variability into the model. The noise term evolves over time:

$$N(t+1) = (1 - \alpha_{\text{noise}})N(t) + \sqrt{2\alpha_{\text{noise}}}\sigma\mathcal{N}(0, 1), \quad (2)$$

where α_{noise} is the noise decay factor, σ determines the noise amplitude, and $\mathcal{N}(0, 1)$ represents a standard normal distribution.

The membrane states are updated based on the spiking states as:

$$S_{\text{mem}}(t) = \alpha S_{\text{mem}}(t-1) + (1 - \alpha)S(t-1), \quad (3)$$

where α represents the decay factor of the membrane states. The relationship between the value of α and memory maintenance is shown in the appendix (see Appendix A for details).

The spike generation process is defined by:

$$S(t) = \begin{cases} 1, & \text{if } V(t) \geq \theta, \\ 0, & \text{otherwise,} \end{cases} \quad (4)$$

where θ is the firing threshold. After a spike is emitted, the membrane potential is reset to V_{reset} as:

$$V(t+1) \leftarrow V_{\text{reset}}. \quad (5)$$

RSNNs in this work utilize the membrane states across all time steps T to compute their output:

$$S_{\text{mem}} = [S_{\text{mem}}(1), S_{\text{mem}}(2), \dots, S_{\text{mem}}(T)]^\top. \quad (6)$$

The predicted output \hat{Y} is then computed as follows:

$$\hat{Y} = \mathbf{W}_{\text{out}} S_{\text{mem}}, \quad (7)$$

where \mathbf{W}_{out} denotes the weights and biases of the output layer.

2.2. Three properties of intrinsic excitability

This work focuses on three types of intrinsic excitability properties, i.e., dendritic time constants α_d , somatic time constants α_s , and firing thresholds θ .

The learnable dendritic time constants α_d enhance signal integration by dynamically weighting inputs across time and frequency domains, enabling the network to balance short-term and long-term features [18, 19, 20]. This work applies the methodology proposed in [21] to the vanilla RSNN model described in Eq.1, and the membrane potential update is detailed below:

$$V(t) = \alpha_s V(t-1) + (1 - \alpha_s) \left(\sum_d \left[\alpha_d V_d(t-1) + (1 - \alpha_d) (\mathbf{W}_{\text{in},d} X(t) + \mathbf{W}_{\text{rec},d} S_{\text{mem}}(t-1)) \right] + N(t) \right), \quad (8)$$

where d is the dendritic branch index, and $\alpha_d = \exp^{-\Delta t/\tau_d}$ is the decay factor for the learnable dendritic time constant τ_d . The explanation of why learnable dendritic time constants contribute to dynamic integration is provided in the appendix (see Appendix B for details).

The learnable soma time constant α_s , defined in Eq.8, is continuously updated during learning. This process ensures temporal fidelity by adaptively controlling the decay of the neuron's membrane potential, effectively balancing fast and slow dynamics across timescales [22].

Finally, learnable firing thresholds θ facilitate complex decision-making by dynamically controlling neuron excitability [23, 24, 25]. By adjusting θ , neurons adaptively shift decision boundaries, enabling the network to effectively separate complex patterns and suppress irrelevant signals.

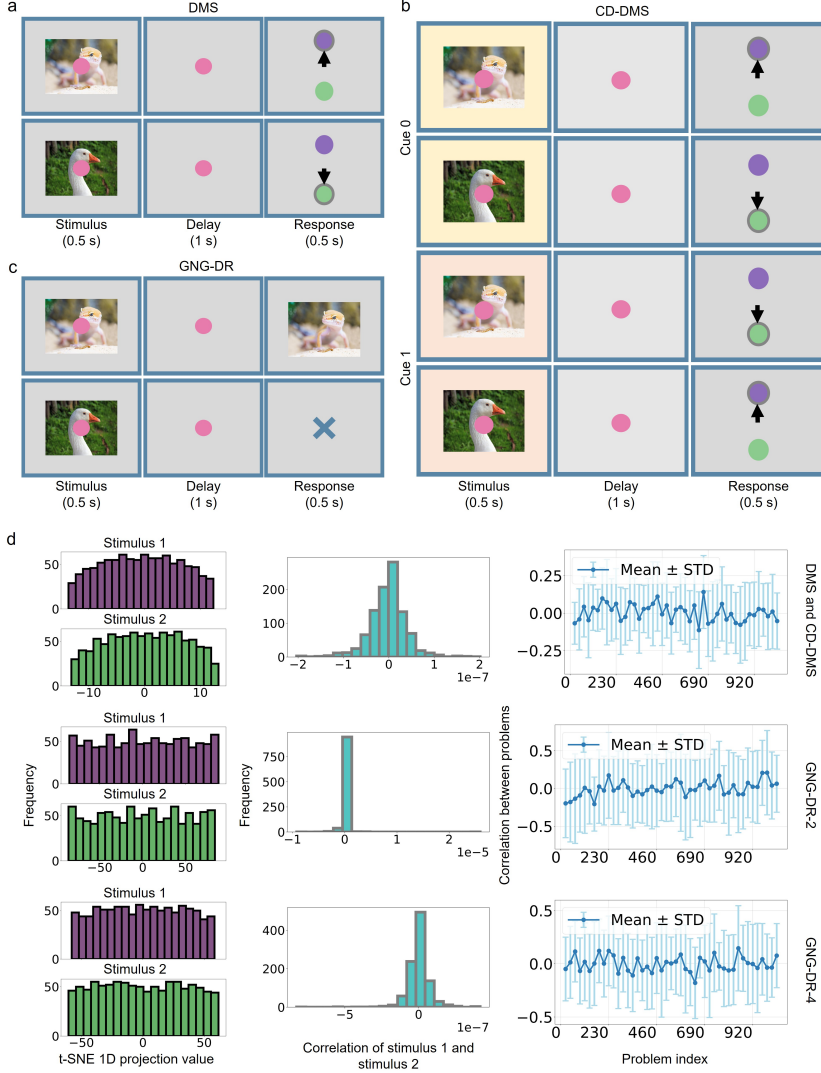


Figure 1: Cognitive tasks and corresponding statistical results. **a** | Cognitive task named Delayed Match-to-Sample (DMS). **b** | The proposed cognitive task named Context-Dependent Delayed Match-to-Sample (CD-DMS). **c** | The proposed cognitive task named Go/No-Go Delayed Recall (GNG-DR). **d** | Statistical results from the data of 1000 problems across four tasks. To facilitate the feature distribution analysis, we reduce the stimulus dimensionality to 1D using the t-SNE method [26]. The CD-DMS and DMS tasks yield identical statistical results because the stimuli in CD-DMS differ only by the inclusion of additional cue features

3. Methods

3.1. Schema learning framework

Inspired by the approach proposed in [11], we develop a generalized framework for schema learning, as shown in Algorithm 1. This framework simulates schema learning in the brain driven by natural dynamics and supports various cognitive tasks.

Specifically, for each problem p within the specified task T , the function DataGen generates data (X_p, Y_p) , which is then used for iterative optimization of the model M via gradient descent. Meanwhile, the framework evaluates performance by tracking loss trends $loss_history$ and checking convergence against a predefined threshold C . The framework marks problems as successfully learned when the model meets the criterion and triggers early stopping after N_{fail} consecutive failures. Ultimately, it returns a learned model. The model is considered to have learned the task schema only if it successfully learns all N problems in task T and exhibits a decreasing trend in stopping iterations.

3.2. Schema learning tasks

Building on the schema learning framework, we extend the Delayed Match-to-Sample (DMS) task used in the work [11] with three additional cognitive tasks: CD-DMS, GNG-DR-2, and GNG-DR-4, enabling a systematic investigation of schema mechanisms, as Fig. 1(a-c) shown.

The DMS task adopts the configuration described in [11] and consists of three distinct periods: a 500 ms stimulus period with a 10-dimensional sample input and a 1-dimensional fixation input; a 1000 ms delay period with no visible input; and a 500 ms response period during which the model identifies the stimulus from two alternatives. This task requires the model to integrate multi-dimensional stimuli and process associative memory.

The proposed CD-DMS task extends the DMS task by introducing a context cue in the stimulus period. When the cue is 0, the stimulus-alternative mapping remains unchanged, while a cue of 1 reverses it. Compared to DMS, CD-DMS requires processing more complex associative memory mappings and handling more intricate input integration.

The two proposed GNG-DR tasks are based on DMS but feature a redesigned response period that involves go or no-go decisions. If the model makes a go decision, it needs to generate a recall by reproducing the stimulus values of the samples. Conversely, if the model makes a no-go decision, it

Algorithm 1: Schema Learning Framework

Input: T : Task type, N : Problem number, M : Model, C : Convergence criterion, I_{max} : Max iterations, I_{min} : Min iterations, N_{fail} : Failure threshold

Output: Learned model M

```
1  $p \leftarrow 0$  ;                                // Initialize problem index
2  $fail\_count \leftarrow 0$  ;                      // Initialize failure count
3 while  $p < N$  do
4    $(X_p, Y_p) \leftarrow \text{DataGen}(T, p)$  ;    // Generate problem data
5    $iter \leftarrow 0$  ;                            // Initialize iteration count
6    $loss\_history \leftarrow []$  ;                  // Track loss history
7    $success \leftarrow \text{False}$  ;                // Success flag
8   while True do
9      $loss \leftarrow L(M(X_p), Y_p)$  ;          // Compute loss
10     $loss\_history.append(loss)$  ;            // Record loss
11    if  $iter \geq I_{min}$  then
12       $recent\_avg \leftarrow \text{Mean}(loss\_history[-I_{min} :])$  ; // Avg loss
13    else
14       $recent\_avg \leftarrow \infty$  ;           // Insufficient iterations
15    if  $recent\_avg < C$  then
16       $success \leftarrow \text{True}$  ;           // Mark as successful
17      break ;                         // Stop if loss is below threshold
18    if  $iter \geq I_{max}$  then
19      break ;                         // Stop if max iterations reached
20     $\mathbf{W} \leftarrow \mathbf{W} - \eta \nabla_{\mathbf{W}} L(M(X_p), Y_p)$  ; // Update parameters
21     $iter \leftarrow iter + 1$  ;            // Increment iterations
22    if  $success$  then
23       $fail\_count \leftarrow 0$  ;          // Reset failure count
24    else
25       $fail\_count \leftarrow fail\_count + 1$  ; // Increment failure count
26      if  $fail\_count \geq N_{fail}$  then
27        break ;                   // Stop if failure threshold reached
28     $p \leftarrow p + 1$  ;                // Next problem
29 return  $M$  ;                      // Return final model
```

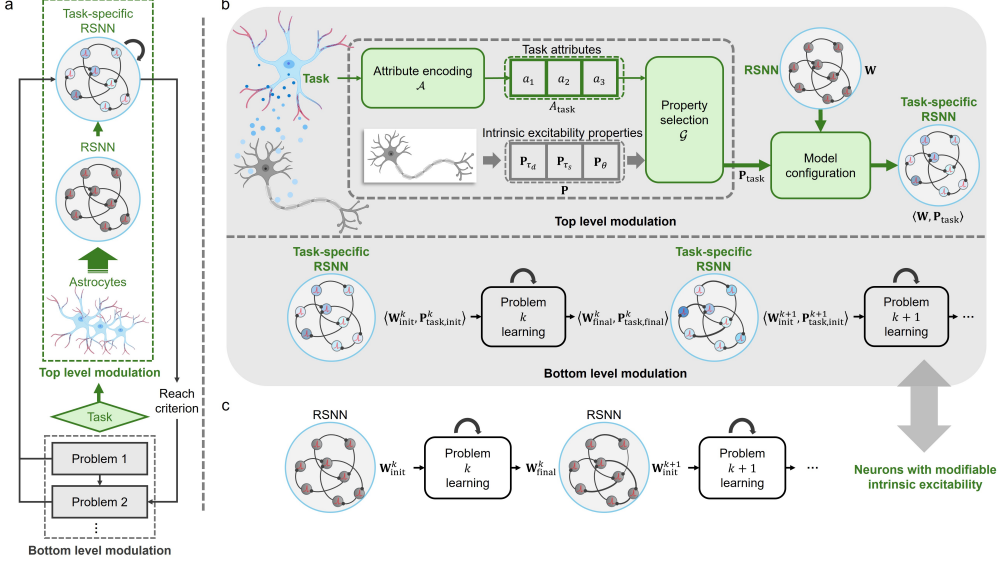


Figure 2: Schematic illustration of recurrent spiking neural networks with hierarchical intrinsic excitability modulation (HM-RSNNs). **a** | Schematic illustration of how two level modulation in HM-RSNNs operates during schema learning. **b** | Schematic illustration of top level and bottom level modulation. The upper part shows top level modulation, and the lower part shows bottom level modulation. **c** | Schematic illustration of schema learning in a traditional RSNN model.

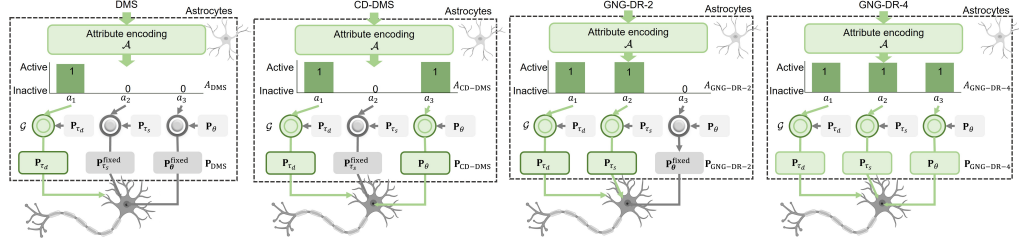


Figure 3: Details of top level modulation across four tasks. Green components indicate activation pathways.

must suppress the response to a value close to 0. Two variants, GNG-DR-2 and GNG-DR-4, are implemented, featuring two-dimensional and four-dimensional stimuli, respectively. Unlike DMS, GNG-DR tasks require temporal fidelity in the second period and memory control (reactivation or inhibition) in the third period, replacing associative memory.

3.3. The proposed method: HM-RSNNs

We propose a biologically plausible model called HM-RSNNs. In contrast to traditional RNN-based approaches, the model employs RSNNs with specialized neurons characterized by hierarchically modulated intrinsic excitability, specifically designed to improve schema learning performance.

Two level modulation during schema learning is shown in Fig. 2(a). The task type is first input into the HM-RSNN model, where top level modulation simulates brain astrocytes to configure task-specific properties, forming a task-specific RSNN. The model then learns intra-task problems sequentially, using bottom level modulation to fine-tune properties and improve learning efficiency. After satisfying a predefined criterion, it proceeds to the next problem.

3.3.1. Top level modulation

Details of the top level modulation are depicted in Fig. 2(b). This process simulates the brain's mechanism of decomposing task attributes upon reception and adapting neuronal properties to diverse task demands, closely linked to astrocytic metaplasticity. Specifically, astrocytes propagate calcium waves to modulate neuronal activity across large-scale networks over relatively slow timescales [27]. This mechanism allows them to indirectly integrate task-relevant contextual information into the functional dynamics of neural circuits [28, 29, 30]. In our work, this mechanism modulates the intrinsic excitability of neurons, determining which properties are adjustable and which remain fixed.

We simplify and formalize these complex modulations into a gating-based mechanism, adjusting intrinsic excitability properties \mathbf{P}_{task} according to task attributes A_{task} :

$$\mathbf{P}_{\text{task}} = \mathcal{G}(A_{\text{task}}, \mathbf{P}) = \langle \mathcal{G}(a_1, \mathbf{P}_{\tau_d}), \mathcal{G}(a_2, \mathbf{P}_{\tau_s}), \mathcal{G}(a_3, \mathbf{P}_{\theta}) \rangle, \quad (9)$$

$$\mathcal{G}(a_i, \mathbf{P}_j) = \begin{cases} \mathbf{P}_j, & \text{if } a_i = 1 \text{ (learnable),} \\ \mathbf{P}_j^{\text{fixed}}, & \text{if } a_i = 0 \text{ (fixed).} \end{cases} \quad (10)$$

In the proposed HM-RSNNs, we focus on three neuronal properties regulated by top level modulation, denoted as \mathbf{P}_j , where $j \in \tau_d, \tau_s, \theta$. Specifically, \mathbf{P}_{τ_d} represents the set of all learnable dendritic time constants, \mathbf{P}_{τ_s} represents the set of all learnable somatic time constants, and \mathbf{P}_{θ} represents the set of all learnable firing thresholds. The gating function $\mathcal{G}(A_{\text{task}}, \mathbf{P})$ maps the task-specific attributes A_{task} to the learnable states of \mathbf{P}_j .

Here, the A_{task} are obtained through the attribute encoding module \mathcal{A} :

$$A_{\text{task}} = \mathcal{A}(I_{\text{task}}), \quad (11)$$

$$A_{\text{task}} = [a_1 \ a_2 \ a_3], \quad (12)$$

Here, I_{task} denotes the input task. The variable $a_1 \in \{0, 1\}$ specifies whether dynamic integration is required for complex inputs, $a_2 \in \{0, 1\}$ indicates the need for temporal fidelity, and $a_3 \in \{0, 1\}$ represents the demand for complex decision-making.

We hand-code four task-specific attributes A_{task} based on specific task demands. All four tasks involve multidimensional stimuli, necessitating complex input integration. Compared to DMS and GNG-DR-2, CD-DMS and GNG-DR-4 impose higher demands on decision-making complexity. Additionally, GNG-DR-2 and GNG-DR-4 require temporal fidelity. The task-specific attribute encodings are outlined as follows:

$$A_{\text{DMS}} = [1 \ 0 \ 0], \quad A_{\text{CD-DMS}} = [1 \ 0 \ 1], \quad (13)$$

$$A_{\text{GNG-DR-2}} = [1 \ 1 \ 0], \quad A_{\text{GNG-DR-4}} = [1 \ 1 \ 1]. \quad (14)$$

Consequently, a gating mechanism activates the adjustability of the corresponding intrinsic excitability properties. Specifically, for the DMS task, only dendritic time constants \mathbf{P}_{τ_d} are learnable, yielding \mathbf{P}_{DMS} . In the CD-DMS task, dendritic time constants \mathbf{P}_{τ_d} and firing thresholds \mathbf{P}_θ are learnable, resulting in $\mathbf{P}_{\text{CD-DMS}}$. In the GNG-DR-2 task, learnable parameters include dendritic time constants \mathbf{P}_{τ_d} and somatic time constants \mathbf{P}_{τ_s} , producing $\mathbf{P}_{\text{GNG-DR-2}}$. Lastly, in the GNG-DR-4 task, dendritic time constants \mathbf{P}_{τ_d} , somatic time constants \mathbf{P}_{τ_s} , and firing thresholds \mathbf{P}_θ are all learnable, resulting in $\mathbf{P}_{\text{GNG-DR-4}}$. Details are provided in Fig. 3 and the following equations:

$$\mathbf{P}_{\text{DMS}} = \langle \mathbf{P}_{\tau_d}, \mathbf{P}_{\tau_s}^{\text{fixed}}, \mathbf{P}_\theta^{\text{fixed}} \rangle, \quad \mathbf{P}_{\text{CD-DMS}} = \langle \mathbf{P}_{\tau_d}, \mathbf{P}_{\tau_s}^{\text{fixed}}, \mathbf{P}_\theta \rangle, \quad (15)$$

$$\mathbf{P}_{\text{GNG-DR-2}} = \langle \mathbf{P}_{\tau_d}, \mathbf{P}_{\tau_s}, \mathbf{P}_\theta^{\text{fixed}} \rangle, \quad \mathbf{P}_{\text{GNG-DR-4}} = \langle \mathbf{P}_{\tau_d}, \mathbf{P}_{\tau_s}, \mathbf{P}_\theta \rangle. \quad (16)$$

3.3.2. Bottom level modulation

The details of the bottom level modulation are shown in Fig. 2(b). It represents a distinct form of fast-timescale metaplasticity, differing from astrocytic metaplasticity, and simulating fine-tuning of neuronal properties during intra-task learning to improve learning efficiency.

Biological evidence supports metaplastic fine-tuning of three neuronal properties: dopamine-driven metaplasticity in the striatum adjusts dendritic excitability via D1/D2 receptor signaling for motor regulation [31]; perisomatic biochemical changes enable behavioral adaptations [32]; and D1/D5 receptor activation in the hippocampus lowers long-term potentiation thresholds in subiculum neurons, facilitating the differentiation of novel and familiar information for downstream processing [33].

We simplify bottom level modulation by integrating neuronal property adjustments into the gradient descent process. Our HM-RSNNs jointly update weights \mathbf{W} and intrinsic excitability properties \mathbf{P}_{task} , leveraging both for subsequent problems. Specifically, during problem k training, our HM-RSNNs refine $\mathbf{W}_{\text{task}}^k$ and $\mathbf{P}_{\text{task}}^k$, then transfer $\langle \mathbf{W}_{\text{task,final}}^k, \mathbf{P}_{\text{task,final}}^k \rangle$ to initialize problem $k + 1$:

$$\langle \mathbf{W}_{\text{task,init}}^{k+1}, \mathbf{P}_{\text{task,init}}^{k+1} \rangle = \langle \mathbf{W}_{\text{task,final}}^k, \mathbf{P}_{\text{task,final}}^k \rangle. \quad (17)$$

This modulation enhances the consolidation of task-specific knowledge, thereby promoting faster neural adaptation to future problems. Comparisons with the traditional RSNN model are shown in Fig. 2(b) and Fig. 2(c). The traditional model adjusts only synaptic connection weights \mathbf{W} during intra-task learning, thereby limiting neural plasticity and hindering efficient schema formation.

3.4. Loss functions

The total loss includes a base loss term and additional loss terms. The base loss term $\mathcal{L}_{\text{Base}}$ is defined as cross-entropy (CE) for DMS and CD-DMS tasks, and mean squared error (MSE) for GNG-DR-2 and GNG-DR-4 tasks. The additional loss terms serve to regularize model parameters and constrain hidden states, enhancing generalization and stability. Each additional loss term is defined as follows:

$$\mathcal{L}_h = \left| \frac{1}{H} \sum_{h=1}^H h_h^2 - \sigma_h^2 \right|, \quad (18)$$

$$\mathcal{L}_{\mathbf{W}_{\text{in}}} = \frac{1}{|\mathbf{W}_{\text{in}}|} \sum_{i,j} \mathbf{W}_{\text{in},ij}^2, \quad (19)$$

$$\mathcal{L}_{\mathbf{W}_{\text{rec}}} = \frac{1}{|\mathbf{W}_{\text{rec}}|} \sum_{i,j} \mathbf{W}_{\text{rec},ij}^2, \quad (20)$$

Task Configuration				
	DMS	CD-DMS	GNG-DR-2	GNG-DR-4
Sample/Fixation Dimension	10/1	11/1	2/1	4/1
Response/Fixation Dimension	2/1	2/1	2/1	4/1
Stimulus/Delay/Response Duration (ms)			500/1000/500	
Schema Learning Configuration				
Number of Problems	1000			
Maximum Iterations per Problem	5000			
Minimum Iterations per Problem	50			
Consecutive Failure Threshold for Early Stopping	3			
Convergence Threshold	0.005 (DMS, CD-DMS, GNG-DR-2) / 0.006 (GNG-DR-4)			
Model Training Configuration				
Learning Rate (RNNs/RSNNs)	0.0001/0.01			
Optimizer	Adam			
β_1 (RNNs/RSNNs)	0.3/0.1			
β_2 (RNNs/RSNNs)	0.999/0.3			
λ_h (RNNs/RSNNs)	0.0005/0.0005			
λ_{in} (RNNs/RSNNs)	0.001/0.001			
λ_{rec} (RNNs/RSNNs)	0.0001/0.0001			
λ_{out} (RNNs/RSNNs)	0.00001/0.1			
α (RNNs/RSNNs)	0.01/0.01			
α_{noise} (RNNs/RSNNs)	0.5/0.5			
σ (RNNs/RSNNs)	0.05/0.05			

Table 1: The standard experimental configuration. RSNNs in this table denote all types of RSNN models used in this work. Moreover, β_1 and β_2 represent the decay rates of the first and second moments in the Adam optimizer [34].

$$\mathcal{L}_{\mathbf{W}_{out}} = \frac{1}{|\mathbf{W}_{out}|} \sum_{i,j} \mathbf{W}_{out,ij}^2. \quad (21)$$

Here, H denotes the number of hidden units, h_h represents the value of the h -th hidden state, and σ_h^2 is the target mean squared value for the hidden states, initially set to 0. Upon switching to the subsequent problem, σ_h^2 is updated based on the previous hidden states. $|\mathbf{W}_{in}|$, $|\mathbf{W}_{rec}|$, and $|\mathbf{W}_{out}|$ denote the number of elements in the input, recurrent, and output weight matrices, respectively.

The total loss is expressed as follows:

$$\mathcal{L} = \mathcal{L}_{Base} + \lambda_h \mathcal{L}_h + \lambda_{in} \mathcal{L}_{\mathbf{W}_{in}} + \lambda_{rec} \mathcal{L}_{\mathbf{W}_{rec}} + \lambda_{out} \mathcal{L}_{\mathbf{W}_{out}}, \quad (22)$$

where λ_h , λ_{in} , λ_{rec} , and λ_{out} are hyperparameters that control the weights of each additional loss term.

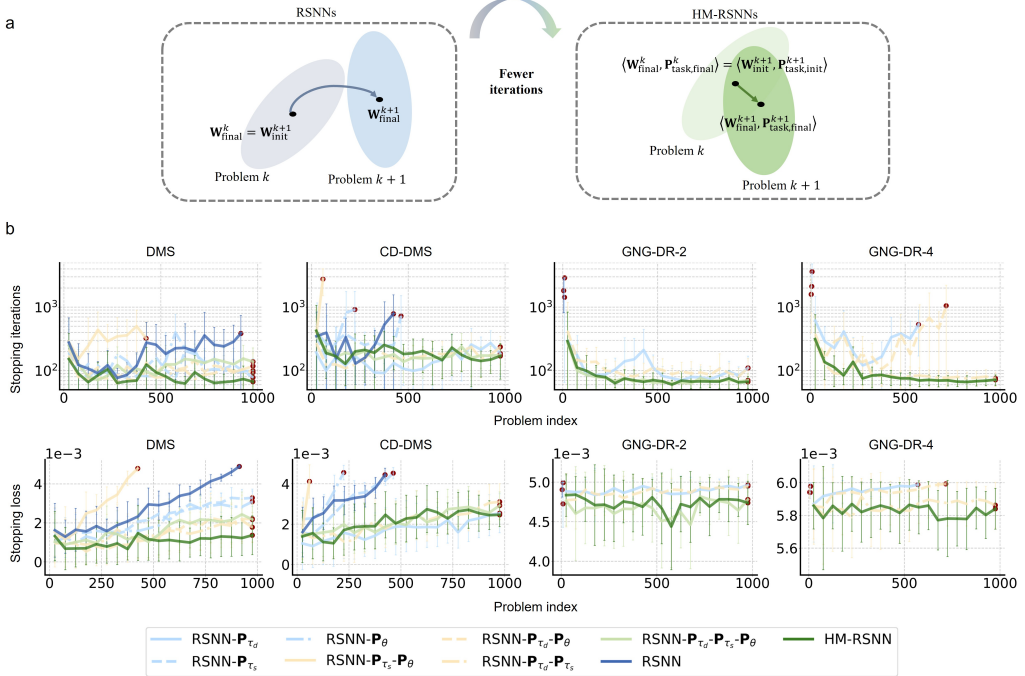


Figure 4: Results of HM-RSNNs across four schema tasks and their comparison with vanilla RSNNs and other RSNN variants. **a** | Schematic illustration of key factors behind HM-RSNNs’ good performance. **b** | Performance comparison among the proposed HM-RSNNs, vanilla RSNNs, and RSNN variants with bottom level modulation. Seven RSNN variants with bottom level modulation are evaluated. In particular, RSNN- \mathbf{P}_{τ_d} represents a variant where \mathbf{P}_{τ_d} is adjusted during intra-task learning, with other variants defined similarly. Results from 1000 problems are grouped into 20 bins to compute the mean and variance, with error bars representing these values. A red circle marks the index of the stopping problem in the corresponding bin when three consecutive problems remain unsolved. Stopping iterations and loss are used as metrics for schema learning performance and problem-solving capacity. Here, the gradual decrease in stopping iterations reflects the progressive formation of schemas, enabling the model to learn more efficiently. By contrast, a prolonged increase in stopping loss indicates rapid saturation of the model, which limits model’s capacity to solve additional problems.

4. Results

4.1. Experimental setup

To ensure reproducibility and biological interpretability, we detail the model initialization process and provide the biological evidence supporting these methods. Specifically, the learnable time constants \mathbf{P}_{τ_d} and \mathbf{P}_{τ_s} are

Model Type	Total Learned / Final Index		Mean Stopping Iterations (Last 200 Problems)		Mean Stopping Loss (Last 200 Problems)	
	DMS	CD-DMS	DMS	CD-DMS	DMS	CD-DMS
RNN	1000/1000	930/931	68	-	0.00470	-
Vanilla RSNN	925/925	439/445	-	-	-	-
HM-RSNN (ours)	1000/1000	1000/1000	69 *	152 *	0.00129 *	0.00254
RSNN- \mathbf{P}_{τ_d}	1000/1000	1000/1000	69 *	232	0.00129 *	0.00236 *
RSNN- \mathbf{P}_{τ_s}	1000/1000	475/475	102	-	0.00321	-
RSNN- \mathbf{P}_θ	1000/1000	237/243	98	-	0.00293	-
RSNN- \mathbf{P}_{τ_s} - \mathbf{P}_θ	447/447	59/66	-	-	-	-
RSNN- \mathbf{P}_{τ_d} - \mathbf{P}_θ	1000/1000	1000/1000	108	152 *	0.00213	0.00254
RSNN- \mathbf{P}_{τ_d} - \mathbf{P}_{τ_s}	1000/1000	1000/1000	100	200	0.00192	0.00287
RSNN- \mathbf{P}_{τ_d} - \mathbf{P}_{τ_s} - \mathbf{P}_θ	1000/1000	1000/1000	139	169	0.00220	0.00277

Table 2: Performance comparison of all models on DMS and CD-DMS tasks. The Total Learned / Final Index columns represent the number of problems learned and the index of the stopping problem, which together reflect the model’s learning capacity. The Mean Stopping Iterations columns show the average stopping iterations over the last 200 problems, reflecting the model’s efficiency. The Mean Stopping Loss columns show the average loss over the last 200 problems, reflecting further learning potential. The best performance is marked with *. Models that fail to solve all 1000 problems during training cannot provide summary results for the last 200 problems and are therefore marked with -.

randomly initialized with positive values and normalized using the sigmoid function. This approach results in larger initial decay factors, enhancing stability during early training by enabling smoother input integration and facilitating gradual learning, in line with the biological evidence reported in [35, 36]. The threshold \mathbf{P}_θ is initialized to 0.25. This configuration ensures relatively higher neural excitability during early learning, facilitating quicker adaptation in development, in line with the biological evidence reported in [37, 38, 39].

Additionally, the models comprise 256 neurons, with standard weights initialized as described in [11]. Each neuron includes 2 dendritic branches with sparse connections, following the setup in [21]. Finally, the basic configuration is detailed in Table 1.

4.2. Task data statistics

For each schema task, we statistically analyze the data from 1000 problems generated by the framework. Data features are uniformly sampled across the feature space, as shown in Fig. 1(d), column 1. The two stimuli within each problem are orthogonal, indicating that they are uncorrelated

Model Type	Total Learned / Final Index		Mean Stopping Iterations (Last 200 Problems)		Mean Stopping Loss (Last 200 Problems)	
	GNG-DR-2	GNG-DR-4	GNG-DR-2	GNG-DR-4	GNG-DR-2	GNG-DR-4
RNN	1000/1000	1000/1000	92	101	0.00473 *	0.00583
Vanilla RSNN	3/6	0/0	-	-	-	-
HM-RSNN (ours)	1000/1000	1000/1000	68 *	68 *	0.00477	0.00582 *
RSNN- \mathbf{P}_{τ_d}	999/1000	587/591	93	-	0.00494	-
RSNN- \mathbf{P}_{τ_s}	14/26	7/22	-	-	-	-
RSNN- \mathbf{P}_{θ}	1/10	3/11	-	-	-	-
RSNN- \mathbf{P}_{τ_s} - \mathbf{P}_{θ}	0/0	5/7	-	-	-	-
RSNN- \mathbf{P}_{τ_d} - \mathbf{P}_{θ}	999/1000	727/729	96	-	0.00493	-
RSNN- \mathbf{P}_{τ_d} - \mathbf{P}_{τ_s}	1000/1000	1000/1000	68 *	77	0.00477	0.00588
RSNN- \mathbf{P}_{τ_d} - \mathbf{P}_{τ_s} - \mathbf{P}_{θ}	1000/1000	1000/1000	69	68 *	0.00473 *	0.00582 *

Table 3: Performance comparison of all models on GNG-DR-2 and GNG-DR-4 tasks. Metrics and conventions align with those in Table 2.

and independent, as shown in Fig. 1(d), column 2. Additionally, the data is randomly generated, ensuring no correlation between adjacent problems or problem indices, as shown in Fig. 1(d), column 3.

The distribution characteristics of the data promote diversity, ensure distinguishability between stimuli, and maintain independence across problems, thereby enhancing the methodological rigor of the schema learning paradigm.

4.3. Performance evaluation of HM-RSNNs

The performance of HM-RSNNs is evaluated across four tasks and compared with vanilla RSNNs to highlight the role of hierarchical modulation. Furthermore, comparisons with RSNN variants incorporating different bottom level modulation are conducted for ablation studies.

Vanilla RSNN performance is shown in Fig. 4(b) with blue solid lines. Due to the lack of adjustable intrinsic excitability properties, vanilla RSNNs are unable to solve all 1000 problems in any task. Specifically, for the DMS task, although the vanilla RSNN can solve up to 925 problems, it fails to demonstrate the brain-like ability to learn-to-learn. Instead, its learning curve steepens as the number of problems increases, as shown in Fig. 4(b), column 1. The performance further declines in the more complex CD-DMS task, solving only 439 problems, as shown in Fig. 4(b), column 2, which highlights the model’s difficulty in handling intricate relationships. In the GNG-DR-2 task, the vanilla RSNN solves only 3 problems, while it completely fails in the most demanding GNG-DR-4 task, as shown in Fig. 4(b),

columns 3 and 4, underscoring its inability to maintain memory integrity under challenging conditions.

The performance of RSNN variants incorporating different bottom level modulation is depicted in Fig. 4(c), represented by low-saturation lines. Specifically, the inclusion of \mathbf{P}_{τ_d} improves baseline performance across all tasks by enhancing synaptic integration and associative memory. However, this variant still fails to solve all 1000 GNG-DR problems, indicating limitations in achieving precise temporal fidelity. The variant integrating \mathbf{P}_{τ_s} with \mathbf{P}_{τ_d} successfully solves all 1000 GNG-DR problems. By contrast, variant with \mathbf{P}_{τ_s} alone underperforms the combined configuration, underscoring the synergistic effects of \mathbf{P}_{τ_d} and \mathbf{P}_{τ_s} . The variant with \mathbf{P}_θ offers limited improvement, and its combination with \mathbf{P}_{τ_s} even negatively impacts performance, likely due to increased complexity in excitability dynamics. However, when the variant with \mathbf{P}_θ is combined with \mathbf{P}_{τ_d} , or with both \mathbf{P}_{τ_d} and \mathbf{P}_{τ_s} , it enables the model to learn more complex decision boundaries, improving performance on challenging tasks like CD-DMS and GNG-DR-4.

While some variants with bottom level modulation improve schema learning performance, no single configuration consistently outperforms others across all tasks, emphasizing the importance of top level modulation.

The performance of HM-RSNNs is shown in Fig. 4(b) with green solid lines. It outperforms all other RSNNs across four tasks and exhibits brain-like learn-to-learn capabilities. From a computational perspective, the task-specific configuration of the model and optimization of initialization states facilitate the extraction of shared patterns, leading to the superior performance of HM-RSNNs, as shown in Fig. 4(a). As a supplementary evaluation, we assess all RSNNs on the last 200 problems across four tasks, as shown in Table 2 and Table 3, confirming the superior performance of HM-RSNNs.

4.4. HM-RSNNs: a promising alternative to RNNs

We evaluate the performance of RNNs across four schema tasks and compare them with HM-RSNNs.

On the simpler DMS task, HM-RSNNs achieve comparable performance to RNNs, while RNNs demonstrate greater stability during training. However, on more complex schema tasks, such as CD-DMS, GNG-DR-2, and GNG-DR-4, HM-RSNNs demonstrate significant advantages. Notably, in the CD-DMS task, traditional RNNs fail to solve all 1000 problems, whereas HM-RSNNs succeed. Additionally, in GNG-DR tasks requiring temporal fi-

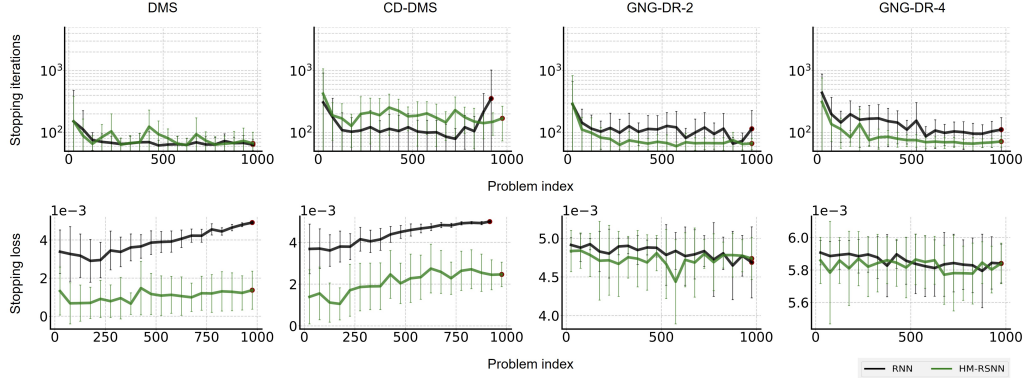


Figure 5: Performance comparison between HM-RSNNs and RNNs across four schema tasks. Metrics and conventions align with those in Fig. 4(b).

delity, HM-RSNNs outperform RNNs in both training stability and overall performance, as shown in Fig. 5.

Building on these findings, we visualize the outputs at problem index 500 across the four tasks, as shown in Fig. 6(a). Compared to RNNs, HM-RSNNs exhibit more precise control over the three task periods (stimulus, delay, response). Notably, HM-RSNNs manage abrupt output changes during two-stage switching more effectively, whereas RNNs exhibit premature state transitions. Additionally, in the GNG-DR-2 and GNG-DR-4 tasks, RNNs struggle with stability and precision, while HM-RSNNs consistently outperform them.

To further explore these dynamics, we visualize the low-dimensional manifolds at problem index 500 across the four tasks. HM-RSNNs exhibit more pronounced transitions in the low-dimensional manifold space, as illustrated in Fig. 6(c).

Overall, these findings highlight the advantage of abrupt state transitions offered by HM-RSNNs, suggesting they are better suited for tasks requiring adaptation to dynamic environments compared to traditional RNNs. A schematic illustration is shown in Fig. 6(b).

The theoretical proof of RNN limitations is provided in the appendix (see Appendix C for details).

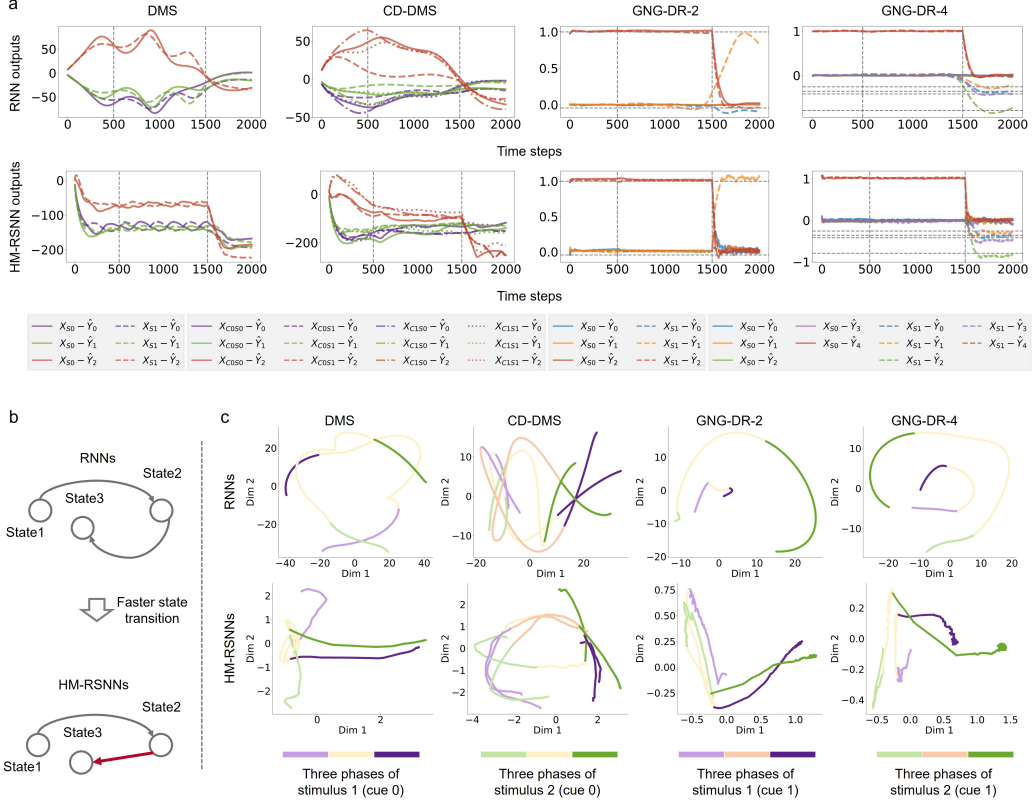


Figure 6: Performance comparison between HM-RSNNs and RNNs. **a** | Output comparison between RNNs and HM-RSNNs on problem 500. Here, X_{S0} and X_{S1} represent the inputs of stimuli 1 and 2, respectively. Similarly, X_{C0S0} and X_{C1S0} correspond to the inputs of stimulus 1 with cues 0 and 1, respectively, with the same notation applied to other combinations. \hat{Y}_i denotes the i -th output value of the model. Horizontal dashed lines indicate the values of stimuli in the GNG-DR tasks. **b** | Schematic illustration of HM-RSNN advantages. **c** | Comparison of low-dimensional manifolds between RNNs and HM-RSNNs on problem 500. PCA [40] is used to map the states of 256 neurons to a two-dimensional representation.

4.5. Neural dynamics in schema learning

4.5.1. Evolution of intrinsic excitability

To explore the evolution of intrinsic excitability across four schema tasks, we record three intrinsic excitability properties (\mathbf{P}_{τ_d} , \mathbf{P}_{τ_s} , and \mathbf{P}_θ) of HM-RSNNs over 1000 problems. The visualization is shown in Fig. 7.

In all four tasks, the evolution follows consistent patterns. Specifically, the distribution of \mathbf{P}_{τ_d} is initially concentrated around 1 and gradually transitions

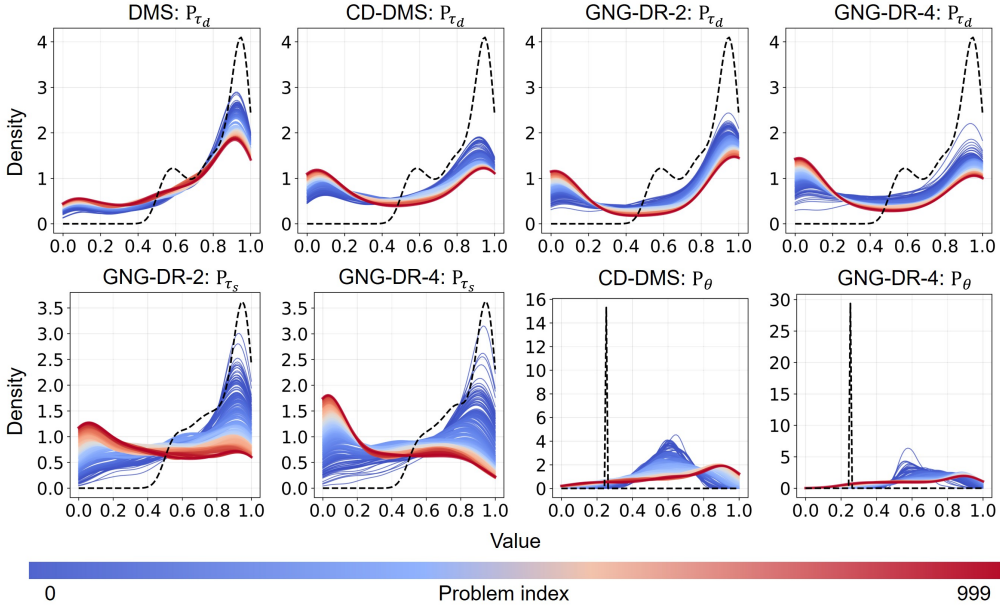


Figure 7: Intrinsic excitability evolution during schema learning. All properties are analyzed after normalization. The first row shows the evolution of the \mathbf{P}_{τ_d} density distribution across DMS, CD-DMS, GNG-DR-2, and GNG-DR-4 tasks. The second row depicts the dynamics of \mathbf{P}_{τ_s} in GNG-DR-2 and GNG-DR-4 tasks, as well as \mathbf{P}_θ in CD-DMS and GNG-DR-4 tasks. The dashed lines represent the initial distribution of properties. Small random noise is added to the parameter \mathbf{P}_θ to improve the visibility of the density curve, as \mathbf{P}_θ is initialized to a constant value of 0.25.

into a bimodal shape with peaks around 0 and 1. This transition reflects schema formation, where an increase in low-value \mathbf{P}_{τ_d} facilitates rapid, high-frequency processing, consistent with the demands of schema-driven flexible information integration.

Moreover, in GNG-DR-2 and GNG-DR-4, \mathbf{P}_{τ_s} transitions from a peak near 1 to another near 0. This shift indicates a reallocation of neural resources, with increased emphasis on rapid feature extraction and reduced reliance on long-term memory. Notably, this change parallels the evolution of \mathbf{P}_{τ_d} , further reflecting the schema-driven adaptation to faster processing.

Finally, in CD-DMS and GNG-DR-4, \mathbf{P}_θ evolves into a more uniform distribution, with its peak shifting toward larger values. This indicates a refinement of decision boundaries, enabling the network to handle increasingly complex tasks more effectively.

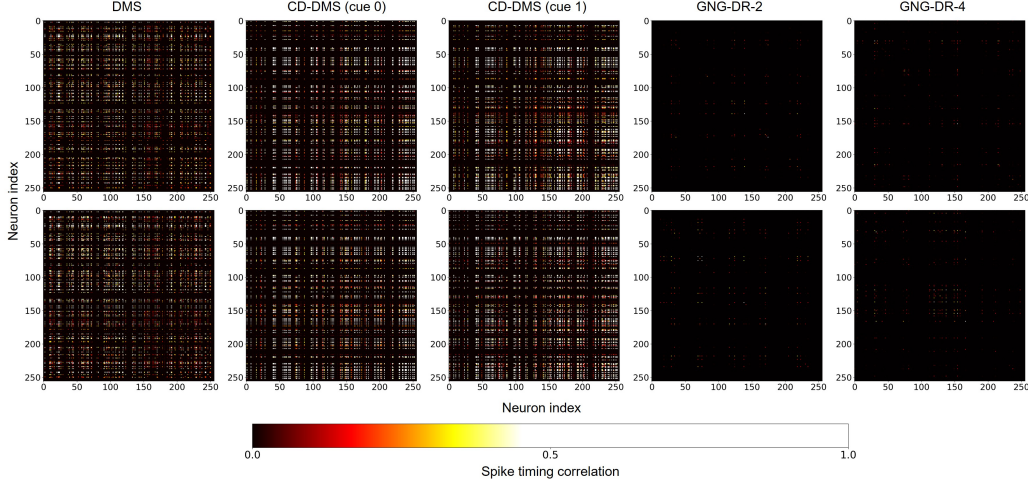


Figure 8: Neural coordination differences of HM-RSNNs across four schema tasks. The correlations are computed and normalized based on spike activities at adjacent time steps. Neural coordination for stimulus 1 is displayed in the top row, whereas neural coordination for stimulus 2 is displayed in the bottom row.

4.5.2. Neural coordination differences

Leveraging the spiking characteristics of the RSNN model, we examine neural coordination by visualizing spike timing correlations among 256 neurons. The visualization results across four tasks are presented in Fig. 8, based on HM-RSNNs trained on the final problem.

Specifically, in DMS and CD-DMS tasks, neural coordination occurs more frequently than in GNG-DR-2 and GNG-DR-4, suggesting that the higher-dimensional input in these tasks requires increased neural coordination. Notably, in CD-DMS, coordination differences between cue 0 and cue 1 surpass those observed between different stimuli. Additionally, in GNG-DR tasks, go decisions enhance coordination, emphasizing the role of neural coordination in precise memory recall and maintenance.

All these findings suggest that the discrepancies observed are largely governed by higher-level task rules, with minimal contribution from stimulus-specific features.

4.5.3. Distribution of intrinsic excitability in different schemas

To explore the distribution of intrinsic excitability within schemas, we simulate biological lesion experiments by selectively ablating neural subsets

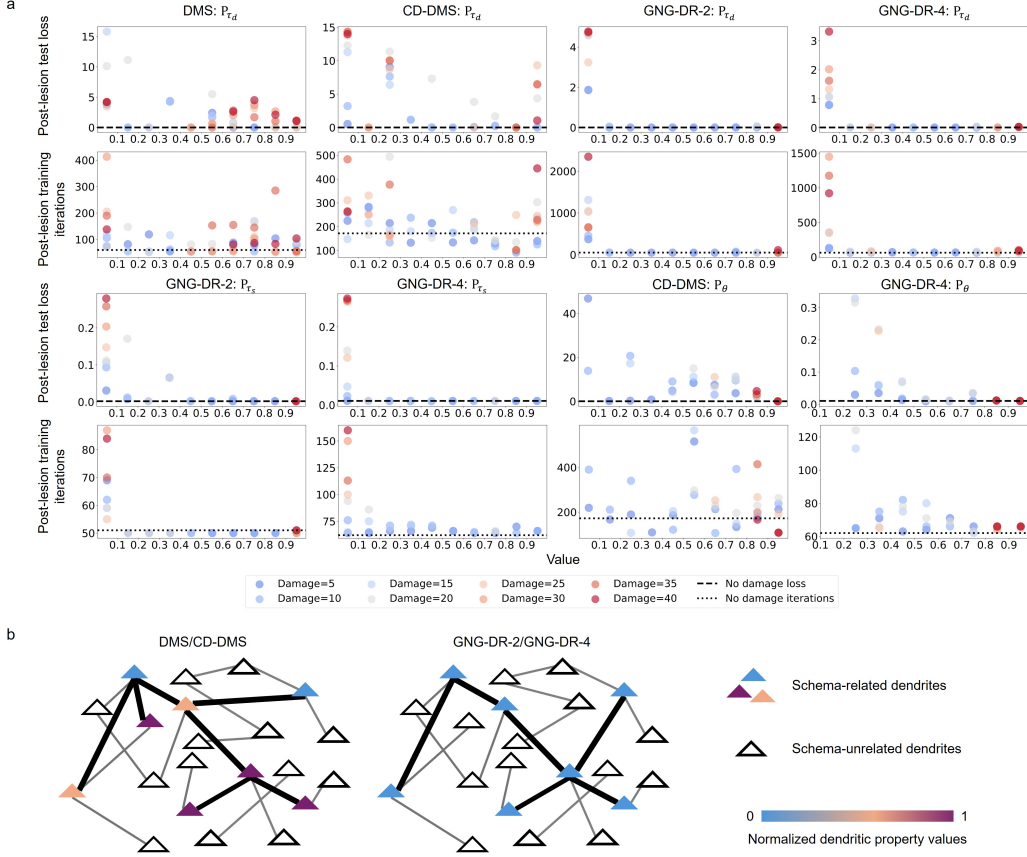


Figure 9: Lesion analyses across four schema tasks. **a** | Post-lesion testing and training of HM-RSNNs across four tasks. The lesion procedure is applied to the model trained on problem 998. Post-lesion testing is conducted on the same problem, while post-lesion training is initiated at problem 999. To configure the lesions, we normalize the three intrinsic excitability properties, divide each into ten bins, and adjust the number of damaged subsets in each bin accordingly. Neurons are damaged by blocking spiking activities for \mathbf{P}_{τ_s} and \mathbf{P}_θ , and by disrupting dendritic computation for \mathbf{P}_{τ_d} . **b** | Schematic illustration of the \mathbf{P}_{τ_d} distribution across different schema tasks. Specifically, GNG-DR tasks rely on dendritic branches characterized by short time constants, whereas DMS and CD-DMS utilize dendritic branches with both short and long time constants.

within specified property bin intervals. The post-lesion test loss measures the importance of the ablated subsets in task information representation, while the post-lesion training iterations measure their contribution to schemas. The results of lesion experiments are shown in Fig. 9a.

Specifically, ablating subsets in the 0-0.1 \mathbf{P}_{τ_d} bin significantly increases

post-lesion training iterations, suggesting a strong coupling between these subsets and the schema across four tasks. Notably, in GNG-DR tasks, disrupting these subsets results in an order-of-magnitude increase of training iterations, highlighting that the schema is predominantly localized within this range. Conversely, in DMS and CD-DMS tasks, the ablation-induced increase in training iterations is more evenly distributed. These mean that schemas in GNG-DR tasks mainly rely on dendritic branches with short time constants, while schemas in DMS and CD-DMS depend on dendritic branches with both short and long time constants, as shown in Fig. 9(b).

Moreover, our findings reveal a strong correlation between post-lesion training iterations and test loss, as shown in Fig. 9(a), highlighting the critical role of schemas in task information representation. Interestingly, some subsets are specialized for current problem processing alone. For instance, in GNG-DR-2, ablating \mathbf{P}_{τ_s} subsets within the 0–0.1, 0.1–0.2, and 0.3–0.4 bins significantly impairs task performance while having minimal impact on the schema. These findings are consistent with existing evidence of functional modularity [41, 42, 43].

5. Discussion

Our proposed HM-RSNNs simulate and demonstrate how neural systems achieve both adaptability and efficiency across diverse cognitive demands. Hierarchical modulation of intrinsic excitability, in particular, enhances neural system flexibility. For instance, in GNG-DR tasks, which emphasize high-speed decisions and abrupt transitions, the hierarchical modulation mechanism initially makes dendritic time constants adjustable and subsequently fine-tunes them to a short-time bin (0–0.1) to enable rapid, high-frequency processing. By contrast, in DMS and CD-DMS tasks, which prioritize sustained memory retention and stable stimulus-response mappings, the mechanism fine-tunes certain dendritic time constants to longer-time bins, supporting the delay period and cue-based transformations.

Despite these contributions, certain limitations remain. The hand-coded task attributes reduce the model’s adaptability to dynamic or unknown scenarios, and the intrinsic excitability adjustment currently relies on a binary gating mechanism. Future work will explore the potential benefits of implementing smooth modulation strategies to enhance the model’s adaptability and scalability.

6. Conclusion

This study introduces a generalized behavioral paradigm framework for schema learning, incorporating three novel cognitive tasks. By embedding hierarchical intrinsic excitability modulation into RSNNs, we propose a new model, HM-RSNNs, which outperforms other RSNN variants and RNNs. Leveraging the biomimetic properties of HM-RSNNs, we conduct visualization and lesion analyses to uncover intrinsic excitability characteristics and neural coordination during schema learning. This work offers a more biologically plausible alternative to RNNs and provides key insights into biologically inspired computation, bridging artificial and biological systems.

CRediT authorship contribution statement

Yingchao Yu: Writing – original draft, Writing – review & editing, Software, Methodology, Formal analysis. **Yaochu Jin:** Writing – review & editing, Supervision, Resources, Methodology, Conceptualization. **Yuchen Xiao:** Writing – review & editing, Methodology. **Yuping Yan:** Writing – review & editing.

Declaration of competing interest

The authors declare no competing financial interests or personal relationships that could have influenced the work reported in this paper.

Acknowledgments

The authors would like to thank Westlake University for providing technical guidance and computational resources. Their support has been instrumental in facilitating the experiments and analyses presented in this paper.

Data availability

Data will be made available on request.

Appendix A. Memory maintenance on membrane states

Expanding Eq.3 recursively, the current membrane state for neuron n can be expressed as:

$$S_{\text{mem},n}(t) = \alpha_n^t S_{\text{mem},n}(0) + \sum_{k=0}^{t-1} \alpha_n^k (1 - \alpha_n) S_n(t - k), \quad (\text{A.1})$$

where $S_{\text{mem},n}(t)$ represents a weighted sum of all historical spiking states $S_n(t - k)$. As $\alpha_n \rightarrow 1$, long-term information is preserved by maintaining contributions from earlier time steps. By contrast, as $\alpha_n \rightarrow 0$, recent inputs dominate, allowing the neuron to adapt to fast-changing dynamics. In this work, α_n is set to 0.01 to enable timely responses across the three periods.

Appendix B. Learnable dendritic time constants for dynamic integration

Learnable dendritic time constants enhance the feature integration by dynamically weighting input signals in time and frequency domains.

In discrete time steps, dendritic branches integrate input signals with learnable time constants τ_d as:

$$V^{\text{total}}(t+1) = \sum_d \sum_{t'=0}^t \exp^{-\frac{t-t'}{\tau_d}} (\mathbf{W}_{\text{in}}^d X(t') + \mathbf{W}_{\text{rec}}^d S_{\text{mem}}(t' - 1)) + N(t). \quad (\text{B.1})$$

Here, τ_d controls the weighting of past time steps t' . Larger τ_d retains long-term memory by emphasizing earlier inputs, while smaller τ_d prioritizes recent signals for short-term memory.

In the frequency domain, τ_d determines the response of each branch to varying frequencies f . The gain of a single branch is:

$$H_d(f) = \frac{1}{1 + j2\pi f \tau_d}, \quad (\text{B.2})$$

where smaller τ_d favors high frequencies, and larger τ_d favors low frequencies. The total frequency response is:

$$H_{\text{total}}(f) = \sum_d H_d(f) = \sum_d \frac{1}{1 + j2\pi f \tau_d}. \quad (\text{B.3})$$

This multi-branch response enables the model to act as a dynamic filter, adapting to complex signals across a wide frequency range and enhancing its ability to process diverse temporal patterns.

Appendix C. Proof of RNN limitations

The dynamics of RNNs are defined as:

$$S(t) = \phi(\mathbf{W}_{\text{in}}X(t) + \mathbf{W}_{\text{rec}}S_{\text{mem}}(t-1) + N(t)), \quad (\text{C.1})$$

where $S(t)$ represents the instantaneous outputs of the RNN neurons. The memory states $S_{\text{mem}}(t)$ are updated according to:

$$S_{\text{mem}}(t) = \alpha S_{\text{mem}}(t-1) + (1-\alpha)S(t), \quad \alpha \in (0, 1], \quad (\text{C.2})$$

with \mathbf{W}_{in} and \mathbf{W}_{rec} as weight matrices, $X(t)$ as the external input, and $N(t)$ as a noise term. The activation function ϕ is defined as the Softplus function:

$$\phi(x) = \frac{1}{\beta} \log(1 + \exp^{\beta x}), \quad (\text{C.3})$$

where $\beta = 1$ by default. The Softplus function is continuous, strictly increasing, and has a bounded first derivative under this configuration.

Starting from Eq.C.2, we have:

$$S_{\text{mem}}(t+1) = \alpha S_{\text{mem}}(t) + (1-\alpha)S(t+1), \quad (\text{C.4})$$

$$S_{\text{mem}}(t) = \alpha S_{\text{mem}}(t-1) + (1-\alpha)S(t). \quad (\text{C.5})$$

Subtracting Eq.C.5 from Eq.C.4 yields:

$$\Delta S_{\text{mem}}(t+1) = \alpha \Delta S_{\text{mem}}(t) + (1-\alpha) \Delta S(t+1), \quad (\text{C.6})$$

where the memory state difference is defined as $\Delta S_{\text{mem}}(t) = S_{\text{mem}}(t) - S_{\text{mem}}(t-1)$, and the instantaneous output difference is given by $\Delta S(t+1) = S(t+1) - S(t)$. By taking the absolute values on both sides of Eq.C.6 and applying the triangle inequality, we obtain:

$$|\Delta S_{\text{mem}}(t+1)| \leq \alpha |\Delta S_{\text{mem}}(t)| + (1-\alpha) |\Delta S(t+1)|. \quad (\text{C.7})$$

This result shows that the one-step change in the memory state is directly influenced by the previous memory state difference $|\Delta S_{\text{mem}}(t)|$ and the instantaneous output change $|\Delta S(t+1)|$. Bounding $|\Delta S(t+1)|$ therefore provides a direct constraint on $|\Delta S_{\text{mem}}(t+1)|$.

From the definition of $S(t)$ in Eq.C.1, we have:

$$S(t) = \phi(x_t), \quad S(t+1) = \phi(x_{t+1}), \quad (\text{C.8})$$

where the inputs to the activation function are given by:

$$x_t = \mathbf{W}_{\text{in}}X(t) + \mathbf{W}_{\text{rec}}S_{\text{mem}}(t-1) + N(t), \quad (\text{C.9})$$

$$x_{t+1} = \mathbf{W}_{\text{in}}X(t+1) + \mathbf{W}_{\text{rec}}S_{\text{mem}}(t) + N(t+1). \quad (\text{C.10})$$

By the Mean Value Theorem, there exists some ξ between x_t and x_{t+1} such that:

$$S(t+1) - S(t) = \phi'(\xi)(x_{t+1} - x_t), \quad (\text{C.11})$$

where the derivative of the Softplus function is:

$$\phi'(x) = \frac{1}{1 + \exp^{-x}}. \quad (\text{C.12})$$

Since $0 < \phi'(x) < 1$ for all x , it follows that:

$$|S(t+1) - S(t)| \leq |x_{t+1} - x_t|. \quad (\text{C.13})$$

Thus, the instantaneous output difference satisfies:

$$|\Delta S(t+1)| \leq |x_{t+1} - x_t|. \quad (\text{C.14})$$

If $\Delta S_{\text{mem}}(t)$, prior to an abrupt transition, is constrained to a small value ϵ , then from Eq.C.6, we have:

$$\Delta S_{\text{mem}}(t+1) = \alpha\epsilon + (1 - \alpha)\Delta S(t+1). \quad (\text{C.15})$$

Substituting Eq.C.14 into Eq.C.15, we obtain:

$$|\Delta S_{\text{mem}}(t+1)| \leq \alpha|\epsilon| + (1 - \alpha)|x_{t+1} - x_t|. \quad (\text{C.16})$$

The derivation shows that the memory state update is constrained by the magnitude of input changes.

This proof demonstrates that the bounded derivative of RNN activation functions constrains memory state updates by the magnitude of input changes. This limitation reduces their ability to capture abrupt transitions in input dynamics, often leading to under-responsiveness to sudden changes. By contrast, RSNNs, with their threshold-based spiking mechanisms, are inherently suited to handle abrupt transitions. Their binary responses enable immediate adjustments to input changes, bypassing the limitations of smooth activation derivatives. Additionally, the membrane potential reset ensures sustained sensitivity to subsequent inputs, while their temporal dynamics efficiently capture rapid variations and preserve long-term memory.

References

- [1] M. van Holk, J. F. Mejias, Biologically plausible models of cognitive flexibility: merging recurrent neural networks with full-brain dynamics, *Current Opinion in Behavioral Sciences* 56 (2024) 101351.
- [2] D. Tse, R. F. Langston, M. Kakeyama, I. Bethus, P. A. Spooner, E. R. Wood, M. P. Witter, R. G. Morris, Schemas and memory consolidation, *Science* 316 (2007) 76–82.
- [3] M. T. Van Kesteren, D. J. Ruiter, G. Fernández, R. N. Henson, How schema and novelty augment memory formation, *Trends in neurosciences* 35 (2012) 211–219.
- [4] M. L. Gick, K. J. Holyoak, Schema induction and analogical transfer, *Cognitive psychology* 15 (1983) 1–38.
- [5] J. Zhou, C. Jia, M. Montesinos-Cartagena, M. P. Gardner, W. Zong, G. Schoenbaum, Evolving schema representations in orbitofrontal ensembles during learning, *Nature* 590 (2021) 606–611.
- [6] H. S. Courellis, J. Minxha, A. R. Cardenas, D. L. Kimmel, C. M. Reed, T. A. Valiante, C. D. Salzman, A. N. Mamelak, S. Fusi, U. Rutishauser, Abstract representations emerge in human hippocampal neurons during inference, *Nature* 632 (2024) 841–849.
- [7] V. Samborska, J. L. Butler, M. E. Walton, T. E. Behrens, T. Akam, Complementary task representations in hippocampus and prefrontal cortex for generalizing the structure of problems, *Nature Neuroscience* 25 (2022) 1314–1326.
- [8] A. R. Vaidya, D. Badre, Abstract task representations for inference and control, *Trends in cognitive sciences* 26 (2022) 484–498.
- [9] M. El-Gaby, A. L. Harris, J. C. Whittington, W. Dorrell, A. Bhomick, M. E. Walton, T. Akam, T. E. Behrens, A cellular basis for mapping behavioural structure, *Nature* (2024) 1–10.
- [10] F. Gobet, P. C. Lane, M. Lloyd-Kelly, Chunks, schemata, and retrieval structures: Past and current computational models, 2015.

- [11] V. Goudar, B. Peysakhovich, D. J. Freedman, E. A. Buffalo, X.-J. Wang, Schema formation in a neural population subspace underlies learning-to-learn in flexible sensorimotor problem-solving, *Nature Neuroscience* 26 (2023) 879–890.
- [12] G. Bellec, D. Salaj, A. Subramoney, R. Legenstein, W. Maass, Long short-term memory and learning-to-learn in networks of spiking neurons, *Advances in neural information processing systems* 31 (2018).
- [13] A. Shaban, S. S. Bezugam, M. Suri, An adaptive threshold neuron for recurrent spiking neural networks with nanodevice hardware implementation, *Nature Communications* 12 (2021) 4234.
- [14] W. Ponghiran, K. Roy, Spiking neural networks with improved inherent recurrence dynamics for sequential learning, in: *Proceedings of the AAAI Conference on Artificial Intelligence*, volume 36, 2022, pp. 8001–8008.
- [15] B. Chakraborty, B. Kang, H. Kumar, S. Mukhopadhyay, Sparse spiking neural network: Exploiting heterogeneity in timescales for pruning recurrent snn, *arXiv preprint arXiv:2403.03409* (2024).
- [16] R. Brette, Philosophy of the spike: rate-based vs. spike-based theories of the brain, *Frontiers in systems neuroscience* 9 (2015) 140675.
- [17] L. F. Abbott, B. DePasquale, R.-M. Memmesheimer, Building functional networks of spiking model neurons, *Nature neuroscience* 19 (2016) 350–355.
- [18] T. Branco, M. Häusser, The single dendritic branch as a fundamental functional unit in the nervous system, *Current opinion in neurobiology* 20 (2010) 494–502.
- [19] J. C. Magee, Dendritic integration of excitatory synaptic input, *Nature Reviews Neuroscience* 1 (2000) 181–190.
- [20] F. Zenke, W. Gerstner, S. Ganguli, The temporal paradox of hebbian learning and homeostatic plasticity, *Current opinion in neurobiology* 43 (2017) 166–176.

- [21] H. Zheng, Z. Zheng, R. Hu, B. Xiao, Y. Wu, F. Yu, X. Liu, G. Li, L. Deng, Temporal dendritic heterogeneity incorporated with spiking neural networks for learning multi-timescale dynamics, *Nature Communications* 15 (2024) 277.
- [22] M. E. Hasselmo, The role of acetylcholine in learning and memory, *Current opinion in neurobiology* 16 (2006) 710–715.
- [23] H. K. Titley, N. Brunel, C. Hansel, Toward a neurocentric view of learning, *Neuron* 95 (2017) 19–32.
- [24] G. Daoudal, D. Debanne, Long-term plasticity of intrinsic excitability: learning rules and mechanisms, *Learning & memory* 10 (2003) 456–465.
- [25] J. Triesch, Synergies between intrinsic and synaptic plasticity in individual model neurons, *Advances in neural information processing systems* 17 (2004).
- [26] L. Van der Maaten, G. Hinton, Visualizing data using t-sne., *Journal of machine learning research* 9 (2008).
- [27] J. A. Crowe, A. H. Bazzari, D. A. Nagel, S. G. Sokolovski, E. U. Rafailov, E. J. Hill, R. H. Parri, Astrocytes control up state and slow oscillation periodicity in human cortical networks, *bioRxiv* (2024) 2024–11.
- [28] N. Bazargani, D. Attwell, Astrocyte calcium signaling: the third wave, *Nature neuroscience* 19 (2016) 182–189.
- [29] Z. Ma, T. Stork, D. E. Bergles, M. R. Freeman, Neuromodulators signal through astrocytes to alter neural circuit activity and behaviour, *Nature* 539 (2016) 428–432.
- [30] C. Murphy-Royal, S. Ching, T. Papouin, Contextual guidance: An integrated theory for astrocytes function in brain circuits and behavior, *arXiv preprint arXiv:2211.09906* (2022).
- [31] D. J. Surmeier, J. Ding, M. Day, Z. Wang, W. Shen, D1 and d2 dopamine-receptor modulation of striatal glutamatergic signaling in striatal medium spiny neurons, *Trends in neurosciences* 30 (2007) 228–235.

- [32] M. C. Guzman-Karlsson, J. P. Meadows, C. F. Gavin, J. J. Hablitz, J. D. Sweatt, Transcriptional and epigenetic regulation of hebbian and non-hebbian plasticity, *Neuropharmacology* 80 (2014) 3–17.
- [33] E. Roggenhofer, P. Fidzinski, O. Shor, J. Behr, Reduced threshold for induction of ltp by activation of dopamine d1/d5 receptors at hippocampal ca1–subiculum synapses, *PLoS One* 8 (2013) e62520.
- [34] D. P. Kingma, Adam: A method for stochastic optimization, arXiv preprint arXiv:1412.6980 (2014).
- [35] G. Mongillo, O. Barak, M. Tsodyks, Synaptic theory of working memory, *Science* 319 (2008) 1543–1546.
- [36] R. Gao, R. L. Van den Brink, T. Pfeffer, B. Voytek, Neuronal timescales are functionally dynamic and shaped by cortical microarchitecture, *Elife* 9 (2020) e61277.
- [37] W. Zhang, D. J. Linden, The other side of the engram: experience-driven changes in neuronal intrinsic excitability, *Nature Reviews Neuroscience* 4 (2003) 885–900.
- [38] D. Debanne, Y. Inglebert, M. Russier, Plasticity of intrinsic neuronal excitability, *Current opinion in neurobiology* 54 (2019) 73–82.
- [39] R. Mozzachiodi, J. H. Byrne, More than synaptic plasticity: role of nonsynaptic plasticity in learning and memory, *Trends in neurosciences* 33 (2010) 17–26.
- [40] H. Hotelling, Analysis of a complex of statistical variables into principal components., *Journal of educational psychology* 24 (1933) 417.
- [41] W. J. Johnston, S. Fusi, Modular representations emerge in neural networks trained to perform context-dependent tasks, *bioRxiv* (2024) 2024–09.
- [42] S. Ostoabic, S. Fusi, Computational role of structure in neural activity and connectivity, *Trends in Cognitive Sciences* (2024).
- [43] J. Tanner, L. Coletta, A. Gozzi, R. F. Betzel, et al., Functional connectivity modules in recurrent neural networks: function, origin and dynamics, arXiv preprint arXiv:2310.20601 (2023).